

RESEARCH ARTICLE

COSMOLOGY

A measurement of the Hubble constant from angular diameter distances to two gravitational lenses

Inh Jee^{1*}, Sherry H. Suyu^{1,2,3*}, Eiichiro Komatsu^{1,4}, Christopher D. Fassnacht⁵, Stefan Hilbert^{6,7}, Léon V. E. Koopmans⁸

The local expansion rate of the Universe is parametrized by the Hubble constant, H_0 , the ratio between recession velocity and distance. Different techniques lead to inconsistent estimates of H_0 . Observations of Type Ia supernovae (SNe) can be used to measure H_0 , but this requires an external calibrator to convert relative distances to absolute ones. We use the angular diameter distance to strong gravitational lenses as a suitable calibrator, which is only weakly sensitive to cosmological assumptions. We determine the angular diameter distances to two gravitational lenses, 810^{+160}_{-130} and 1230^{+180}_{-150} megaparsec, at redshifts $z = 0.295$ and 0.6304 . Using these absolute distances to calibrate 740 previously measured relative distances to SNe, we measure the Hubble constant to be $H_0 = 82.4^{+8.4}_{-8.3}$ kilometers per second per megaparsec.

Measurements of extragalactic distances have revealed that the Universe is expanding (1), and the expansion is accelerating (2, 3). The distance-redshift relation is normalized using the Hubble constant H_0 . The value of H_0 has been inferred directly from the distance-redshift relation in the local Universe [e.g., (4, 5)], and indirectly from the cosmic microwave background (CMB) by assuming a cosmological model (6, 7). Some researchers claim that these two determinations do not agree, differing by a formal statistical significance of more than 3σ (8, 9). Various interpretations for this discrepancy have been suggested: e.g., a modification in early Universe

physics (8, 10). Other researchers claim that the tension is not statistically significant: e.g., that the tension is only at the 2.5σ level (11) or less (12). H_0 determinations using galaxy clusters and ages of old galaxies at intermediate redshift [e.g., (13)] are in agreement with the value from the CMB. If confirmed by further measurements, preferably using independent methods, this discrepancy would call for a revision of the standard model of cosmology, Λ cold dark matter (Λ CDM).

There are multiple ways to measure distances in the Universe based on our knowledge of an object whose distance is measured. One of them is the “luminosity distance” D_L , which is defined

on the basis of the relationship between the measured flux F and the known luminosity L of an object; $D_L = \sqrt{L/(4\pi F)}$. Another way to obtain distance is by means of the “angular diameter distance” D , where the measured angular size θ of an object is related to the known physical size of the object r as $D = r/\theta$. Luminosity distances to type Ia supernovae (SNe) can be used to determine H_0 ; however, they provide only relative distances because of uncertainty in their absolute brightness. SNe measurements of H_0 must adopt an external calibrator of the absolute distance scale, which we refer to as an anchor, to fix the overall normalization of the distances to SNe. Existing local distance measurements use Cepheid variable stars, parallaxes, and/or masers as anchors (4), thereby constructing a distance ladder.

We apply an independent method (14) to measure angular diameter distances to strong gravitational lenses. We apply it to two examples at redshift $z = 0.295$ and 0.6304 with time-varying source brightness. Our goal is to use the two absolute distances to anchor the relative distances of SNe, constraining H_0 . If we can determine the absolute distances to $z = 0.295$ and 0.6304 , we can use them to calibrate SNe data over a wider redshift range $0 < z < 1.4$. From this, we aim to determine the expansion rate at $z = 0$, i.e., H_0 . This is an inverse distance ladder method (15, 16).

Gravitational lensing occurs when photons emitted from a background source are deflected by the gravitational potential of a foreground massive object, such as a galaxy. An observer sees photons arriving from different directions at different times in the case of strong lensing, and these form multiple images on the sky. We show images of the two lensing systems, CLASS B1608+656 (17–19) (hereafter B1608+656) and RXS J1131–1231 (20–22) (hereafter RXJ1131–1231) in Fig. 1, A and B, and schematics of the system configurations in Fig. 1C. The foreground galaxy that dominates the deflection is defined as the

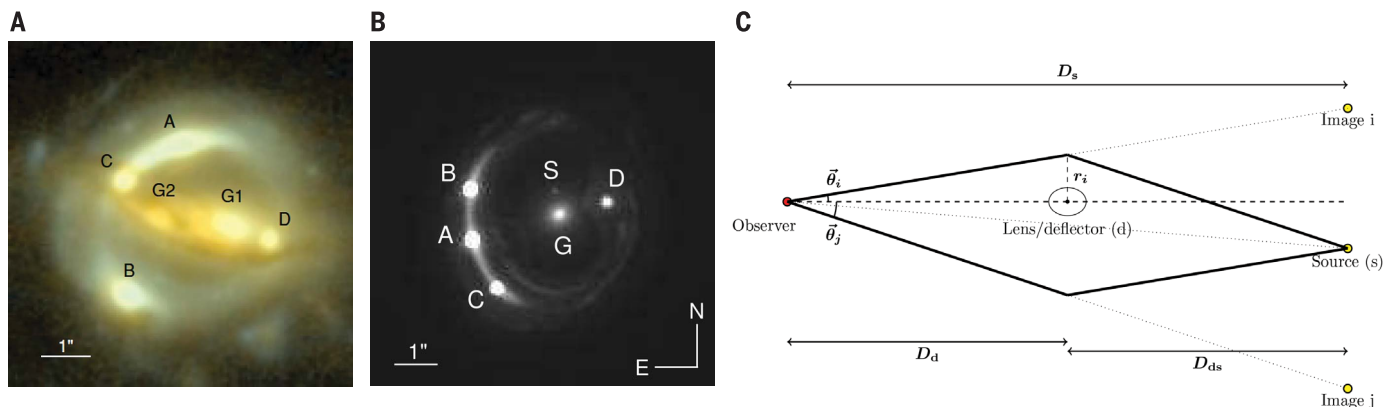


Fig. 1. Images of B1608+656, RXJ1131–1231 and the lensing configuration. Hubble Space Telescope (HST) Advanced Camera for Surveys (ACS) F814W and F606W color composite image of lens B1608+656 (A) and ACS F814W image of RXJ1131–1231 (B) (17, 18, 22). Labels A to D are the quasar images, G1 and G2 are lens galaxies, and S is a satellite galaxy. (C) A schematic diagram of light paths from the source to the observer, forming multiple images. Lensing observables and distances are labeled, where subscripts i and j are the image indices. Panel (A) is reproduced from figure 1 of (28) with permission.

main lens, and the deflections caused by any other structure along the line of sight external to the lens are parameterized by the external convergence, κ_{ext} .

When the source brightness is variable, the arrival time difference between photons from different images (i.e., the time delay) can be measured. Physically, two effects contribute to the difference in photon arrival time: the projected gravitational potential of the enclosed mass, and the difference in geometric path lengths between images, which are summarized as the Fermat potential ϕ . The time delay, Δt , between two images is given by $c\Delta t = D_{\Delta t}\Delta\phi$ (23), where $D_{\Delta t}$ is the time-delay distance $D_{\Delta t} = (1 + z_d)D_d D_s / D_{\text{ds}}$, c is the speed of light, $\Delta\phi$ is the Fermat potential difference between the two images, z_d is the lens/deflector redshift, D is the angular diameter distance, and subscripts “d” and “s” stand for the deflector and the source, respectively (thus, D_{ds} is the angular diameter distance between the deflector and the source). The time-delay distance thus relates ϕ to Δt . The external convergence, κ_{ext} , modifies the relationship between the true $D_{\Delta t}$ and the observed Δt as $c\Delta t = (1 - \kappa_{\text{ext}})D_{\Delta t}\Delta\phi$, where $\Delta\phi$ is the Fermat potential difference based on a model that does not account for the external convergence. Therefore, the true $D_{\Delta t}$ will be scaled by $1/(1 - \kappa_{\text{ext}})$ for an observed (fixed) Δt . Several measurements of H_0 have been reported using $D_{\Delta t}$ alone, which scales inversely to H_0 and weakly depends on other cosmological parameters (20, 24). The latest determination yields $H_0 = 71.9^{+2.4}_{-3.0} \text{ km s}^{-1}\text{Mpc}^{-1}$, which agrees with $H_0 = 73.48 \pm 1.66 \text{ km s}^{-1}\text{Mpc}^{-1}$ from the local distance ladder method (25) but is higher than the CMB result assuming a flat Λ CDM model, $H_0 = 67.4 \pm 0.5 \text{ km s}^{-1}\text{Mpc}^{-1}$ (26). All uncertainties are at the 68% confidence level.

It is possible to measure the angular diameter distance to the deflector, D_d , directly using a simple spherical lens model that relates the radial mass density profile $\rho(r)$ to a radius-independent velocity dispersion σ^2 following $\rho(r) = \sigma^2 / (2\pi G r^2)$ (27), where G is the gravitational constant. The time-delay difference between two images in this model is given by $\Delta t = D_{\Delta t}(\theta_1^2 - \theta_2^2) / (2c)$, where θ_1 and θ_2 are angular positions of the two images (as illustrated in Fig. 1 C). The image positions are related to the

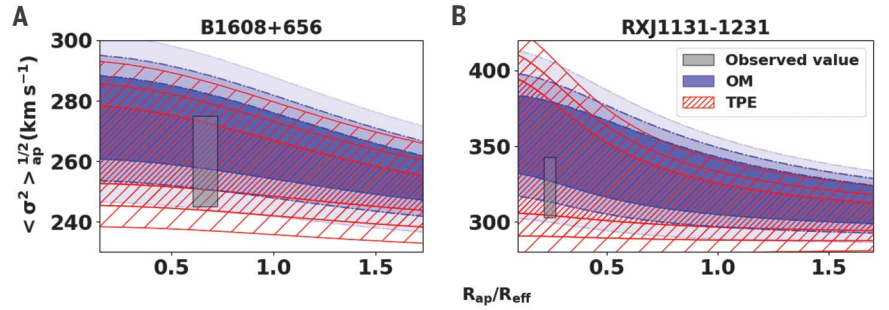


Fig. 2. Predicted velocity dispersion as a function of the aperture size, compared to the observed value. The luminosity-weighted aperture-averaged velocity dispersion for the OM (blue shaded) and TPE (red hatched) anisotropy models are shown, with normalization factors (mass, angular diameter distance, and the Einstein radius) fixed to the best-fitting values. The gray shaded region shows the observed velocity dispersion and the size of the aperture: The vertical position and height of the box show the measurement of the velocity dispersion ($\langle \sigma^2 \rangle^{1/2} = 260 \pm 15$ (19) and $323 \pm 20 \text{ km s}^{-1}$ (22) for each lens, respectively), whereas the horizontal location and width of the box range from the shorter half-width to the longer half-width of the aperture, normalized by the effective radius of the lens galaxy. We vary the slope of the mass profiles γ to 1, 2, and 3σ of the posterior probability distribution (28, 29), shown as the densest to the least-dense shaded areas (A) B1608+656 and (B) RXJ1131-1231. We use flat priors on the anisotropy parameters $r_{\text{ani}} = [0.5, 5]$ (OM) and $\beta_{\text{n,out}} = [-0.6, 0.6]$ (TPE). Our models are compatible with the measurements: The boxes overlap substantially with the 1σ regions.

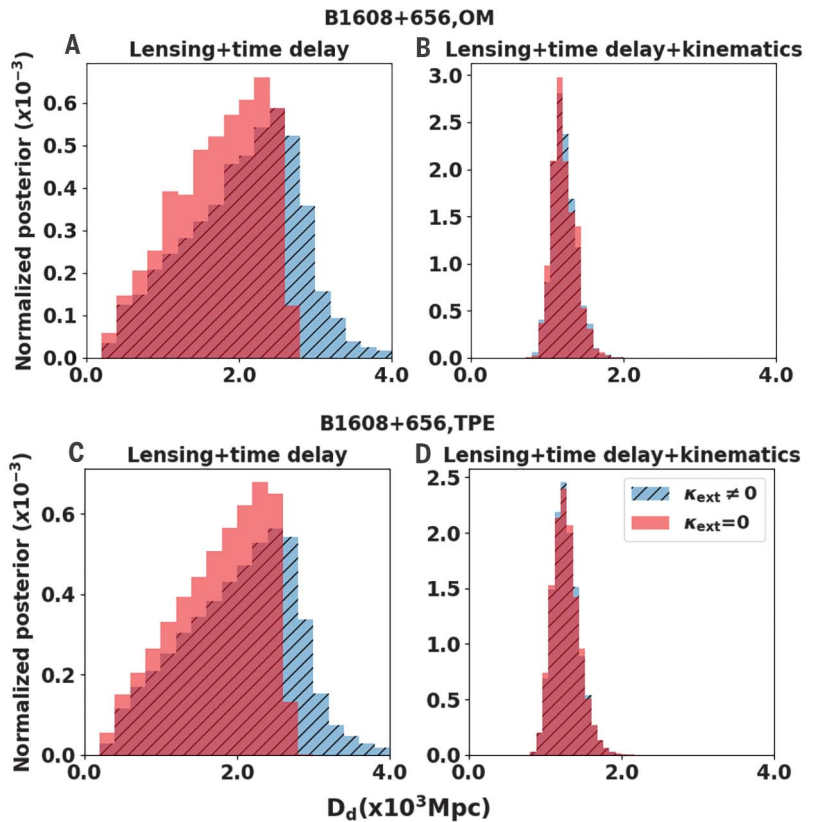


Fig. 3. Normalized posterior probability distributions for the angular diameter distance to the lens B1608+656. (A) and (C) include lensing and time-delay information, whereas (B) and (D) include additionally the kinematics of the lens. The blue-hatched distribution shows the results if the external convergence distribution is estimated by ray-tracing through the Millennium Simulation (36) (fig. S4), whereas the red distribution is the result when the external convergence is set to zero. By including the kinematic information, the angular diameter distance becomes insensitive to κ_{ext} .

¹Max-Planck-Institut für Astrophysik, 85741 Garching, Germany. ²Institute of Astronomy and Astrophysics, Academia Sinica, 11F of Astronomy-Mathematics Building, No.1, Section 4, Roosevelt Road, Taipei 10617, Taiwan.

³Physik-Department, Technische Universität München, 85748 Garching, Germany. ⁴Kavli Institute for the Physics and Mathematics of the Universe, World Premier International Research Center Initiative, Todai Institutes for Advanced Study, the University of Tokyo, Kashiwa 277-8583, Japan.

⁵Physics Department, University of California Davis, Davis, CA 95616, USA. ⁶Exzellenzcluster Universe, 85748 Garching, Germany. ⁷Ludwig-Maximilians-Universität, Universitäts-Sternwarte, 81679 München, Germany. ⁸Kapteyn Astronomical Institute, University of Groningen, 9700 AV Groningen, Netherlands.

*Corresponding author. Email: jee1213@mpa-garching.mpg.de (J.J.); suyu@mpa-garching.mpg.de (S.H.S.)

velocity dispersion as $\sigma^2 = [(\theta_1 + \theta_2)c^2/8\pi]D_s/D_d$. Combining the two, we obtain $D_d = c^3\Delta t/[4\pi\sigma^2(1+z_d)\Delta\theta]$ with $\Delta\theta \equiv \theta_1 - \theta_2$ (27). This expression allows us to determine D_d from measurements of Δt , σ , and $\Delta\theta$. Similar, but more complex, relations hold for more generic lenses with different density profile and velocity structure (14).

The scaling of D_d with Δt , σ^2 , and $\Delta\theta$ can be demonstrated by a qualitative argument. The time delay constrains the projected gravitational potential of the lens within some characteristic size of the system r (e.g., the effective radius of the lens galaxy, where half of the total light emitted from the galaxy is contained) and mass M , $\Delta t \sim GM \ln(r)$, whereas the velocity dispersion of stars in the lens galaxy, σ^2 , constrains the gravitational potential of the lens, $\sigma^2 \sim GM/r$. By combining the two, r is constrained, and by comparing r to the angular separation of lensed images $\Delta\theta$, the lens effectively becomes a ruler, allowing the angular diameter distance to the lens $D_d = r/\Delta\theta \sim \Delta t/(\sigma^2\Delta\theta)$ to be obtained. The physical interpretation of r depends on the lens mass distribution. We adopt the modeling of the lens mass distribution and source light for both of these lensing systems (17, 20, 28); this allows us to use Δt and σ from observations but model the full surface brightness distribution of the lensed source (instead of $\Delta\theta$) in determining D_d . The inference of H_0 from D_d is independent

of κ_{ext} , in contrast to the H_0 inference from $D_{\Delta t}$ that is scaled by $1/(1 - \kappa_{\text{ext}})$ (14, 29).

As $D_d \sim \Delta t/(\sigma^2\Delta\theta)$, the uncertainty on D_d is determined by those on Δt , σ^2 , and $\Delta\theta$; the uncertainty in σ^2 dominates (14). GM/r is determined by the radial component of the stellar velocity dispersion, which is not observable directly. We must assume a three-dimensional structure for the velocity dispersion to relate the observable line-of-sight σ^2 to just the radial component. This velocity anisotropy is the dominant source of uncertainty in this method (14).

Published observations of the lens galaxies provide the velocity dispersion averaged over an aperture of a fixed physical size, which we refer to as the kinematics data. The velocity dispersion of RXJ1131-1231 is estimated by spectroscopy with a rectangular aperture of area 0.81 arc sec by 0.70 arc sec, where the center of the aperture is placed at the center of the lens galaxy. The effective radius of the lens galaxy is $R_{\text{eff}} = 1.85$ arc sec; thus, the half-width of the aperture is $\sim 20\%$ of the effective radius. For B1608+656, $R_{\text{eff}} = 0.58$ arc sec, and $R_{\text{ap}} = 0.84$ arc sec by 1 arc sec, equivalent to $\sim 72\%$ of the effective radius.

In Fig. 2, we illustrate varying sizes of aperture with fixed aspect ratio, to show how non-spherically symmetric velocity dispersion changes the predicted aperture-averaged line-of-sight velocity dispersion, in a power-law mass model where the mass density of the galaxy follows

$\rho(r) \propto r^{-\gamma}$, where γ is the slope of the mass profile. We adopt two parameterized models of the velocity anisotropy, Osipkov-Merritt (OM) (30, 31) and a two-parameter extension (TPE) of OM (32-34). If the aperture had infinite width, the observed velocity dispersion would be the virial limit where the total kinetic energy of a system can be estimated from its total gravitational potential, thus the relation $GM/R \sim \sigma^2$ holds. In this limit, the uncertainty due to the anisotropy is minimized and the difference due to the density profile is the only factor determining the aperture-averaged velocity dispersion (33). The real size of the aperture is a fraction of the effective radius, so the uncertainty due to the anisotropy is larger. Figure 2 shows these uncertainties compared to the measured velocity dispersion as a function of the aperture size (normalized by the effective radius of the galaxy), $R_{\text{ap}}/R_{\text{eff}}$. The TPE model has larger uncertainty than the OM. With the measured uncertainty for the observed velocity dispersions, the difference between the medians of these two anisotropy models is smaller than the statistical uncertainties ($\pm 15 \text{ km s}^{-1}$ for B1608+656, $\pm 20 \text{ km s}^{-1}$ for RXJ1131-1231). The measured velocity dispersion is itself model dependent: e.g., sensitive to a choice of stellar spectral templates (35). This leads to a systematic uncertainty in the velocity dispersion measurement which, in turn, affects the angular diameter distance through $D_d \propto \sigma^{-2}$. This source of systematic uncertainty is taken into account in the velocity dispersion measurements of B1608+656 and RXJ1131-1231.

Figure 3 shows the posterior probability distributions of D_d of B1608+656 estimated using OM and TPE anisotropy models (34), without and with the velocity dispersion information. Although κ_{ext} shifts the posterior probability distribution when the velocity dispersion is not included, the measurement of D_d becomes insensitive to κ_{ext} when it is included (14). This is because the velocity dispersion information (with assumed anisotropy) provides additional constraints on the gravitational potential, which normalizes the angular diameter distance. Figure 4 shows the same posterior probability distributions for RXJ1131-1231.

Our analysis constrains the angular diameter distances to 12 to 20% precision per lens. We marginalize over the uncertainties in anisotropy models by merging two posterior probability distributions of OM and TPE models (34). Our final measurements of the angular diameter distances are $D_d(z = 0.6304) = (1.23^{+0.18}_{-0.15}) \times 10^3 \text{ Mpc}$ for B1608+656, and $D_d(z = 0.295) = (8.1^{+1.6}_{-1.2}) \times 10^2 \text{ Mpc}$ for RXJ1131-1231.

We apply these distances as anchors to the 740 SNe in the Joint Light-curve Analysis [JLA (37)] dataset, allowing us to constrain H_0 and the SNe nuisance parameters (34) simultaneously. We use the MontePython code (38) to perform a Markov chain Monte Carlo analysis. Figure 5 shows the resulting Hubble diagram, i.e., the absolute luminosity distances $D_L = (1+z)^2 D_d$ as a function of redshifts for a flat Λ CDM model. Figure 6 shows the inferred values of H_0 assuming various cosmological models: Λ CDM with flat spatial geometry (f Λ CDM) and

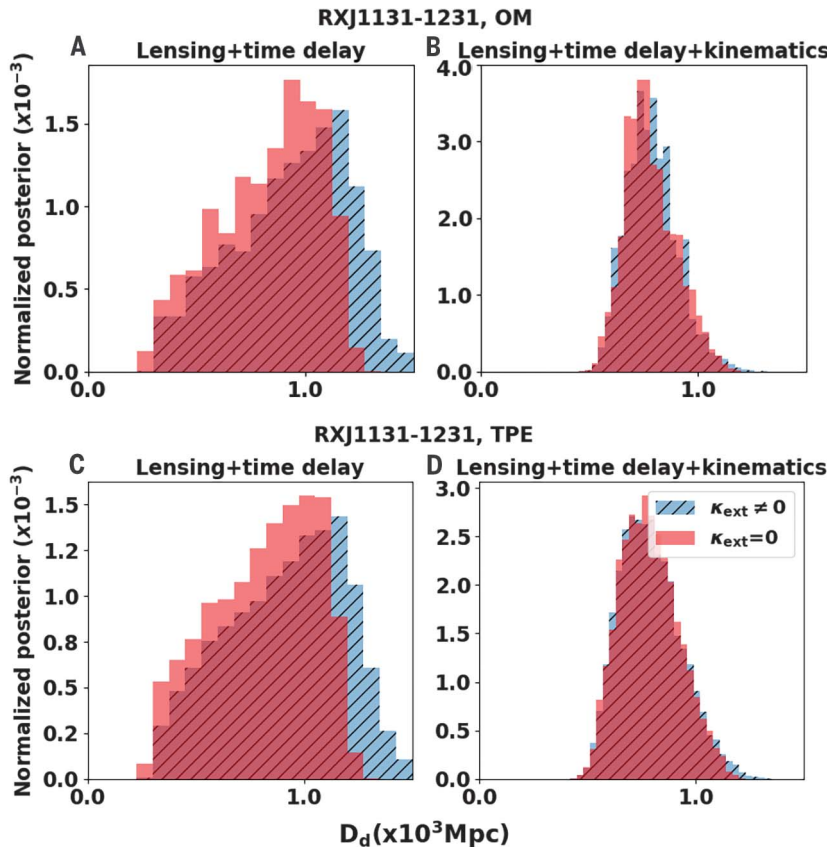
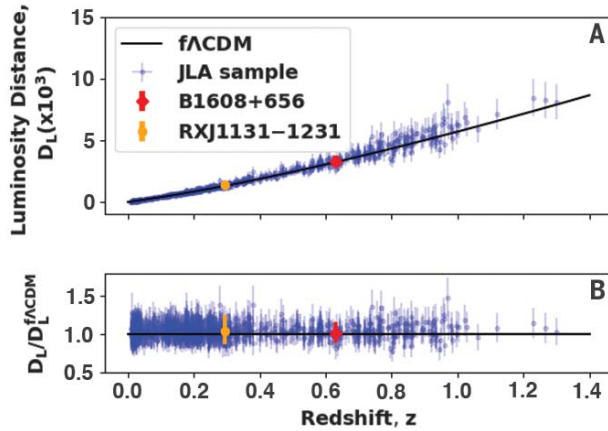


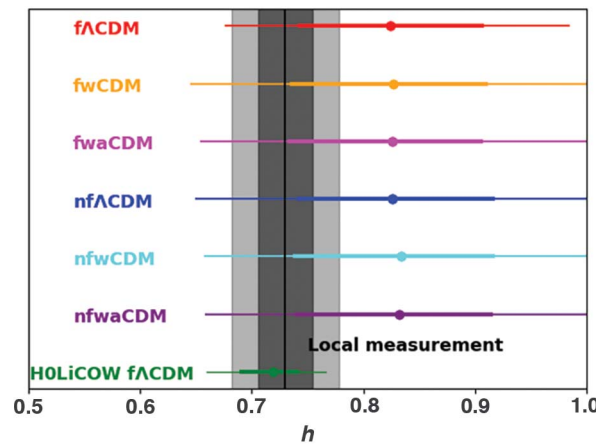
Fig. 4. Same as Fig. 3, but for RXJ1131-1231.

Fig. 5. Hubble diagram.

Derived Hubble diagram (A) and its residuals (B). The blue points with error bars are 740 SNe from JLA (37), normalized by our two lensing distances, shown as an orange and red point. The solid line is the best-fitting flat Λ CDM model.

**Fig. 6. Constraints on the Hubble constant for six cosmological models.**

The gray shaded area is the constraint from the local distance ladder (4), whereas the green line is from three time-delay distances measured by the HOLICOW collaboration (24). The thick and thin solid lines denote the 68% and 95% confidence intervals of the joint fit to the SNe and the D_d data. D_d and $D_{d,t}$ determined from the same lens are not strongly correlated in the case of our two lenses, because the uncertainty in the former is dominated by the kinematics and the latter by κ_{ext} . Therefore, the corresponding constraints on H_0 are nearly independent.



nonflat spatial geometry (nf Λ CDM); a dynamical dark-energy model with flat spatial geometry (fwCDM) and nonflat spatial geometry (nfwCDM), where w is the dark-energy equation of state that characterizes the time evolution of dark-energy density, and w is a parameter in these models; and a dynamical dark-energy model with a time-varying equation of state [$w(z) = w_0 + z w_a / (1+z)$] with flat spatial geometry (fw w_a CDM) and nonflat spatial geometry (nfw w_a CDM), where w_0 and w_a are parameters. By construction, the inverse distance ladder method is insensitive to the assumed cosmological models, which is reflected by the consistent values in Fig. 6. Therefore, we adopt the value for flat Λ CDM, $H_0 = 82.4^{+8.4}_{-8.3}$ km s $^{-1}$ Mpc $^{-1}$ (68% confidence limits) as our fiducial result. We examine and marginalize over uncertainties in the kinematics and mass profiles of the lens galaxies (34). All values of H_0 that we obtain are consistent with H_0 from the distance ladder method (4) and from the time-delay distances (24, 39–41). It is also consistent with, but more precise than, H_0 from the standard siren method (42, 43).

Although our measurement has a larger uncertainty than other direct methods, this is dom-

inated by statistical uncertainty because we use only two lenses to normalize the SNe distances. The precision in our H_0 measurement is presently limited by the number of strong lens systems with measured time delays and ancillary data. Systematic errors, although subdominant, are mainly due to the determination of the velocity structure of the lenses. The single aperture-averaged kinematic measurement and modeling present the main systematic error, which can be overcome by, e.g., spatially resolved kinematic data.

REFERENCES AND NOTES

1. E. Hubble, *Proc. Natl. Acad. Sci. U.S.A.* **15**, 168–173 (1929).
2. S. Perlmutter et al., *Astrophys. J.* **517**, 565–586 (1999).
3. A. G. Riess et al., *Astron. J.* **116**, 1009–1038 (1998).
4. A. G. Riess et al., *Astrophys. J.* **826**, 56 (2016).
5. W. L. Freedman et al., *Astrophys. J.* **758**, 24 (2012).
6. P. A. R. Ade et al., *Astron. Astrophys.* **594**, A13 (2016).
7. Planck Collaboration et al., Planck 2018 results. I. Overview and the cosmological legacy of Planck. arXiv:1807.06205 [astro-ph.CO] (2018).
8. J. L. Bernal, L. Verde, A. G. Riess, *JCAP* **2016**, 019 (2016).
9. W. L. Freedman, *New Astron.* **1**, 0121 (2017).
10. P. Lemos, E. Lee, G. Efsthathiou, S. Gratton, *Mon. Not. R. Astron. Soc.* **483**, 4803–4810 (2019).
11. T. M. C. Abbott et al., *Mon. Not. R. Astron. Soc.* **480**, 3879–3888 (2018).

12. B. R. Zhang et al., *Mon. Not. R. Astron. Soc.* **471**, 2254–2285 (2017).
13. G. P. da Silva, A. G. Cavalcanti, *Braz. J. Phys.* **48**, 521–530 (2018).
14. I. Jee, E. Komatsu, S. H. Suyu, *JCAP* **2015**, 033 (2015).
15. E. Aubourg et al., *Phys. Rev. D Part. Fields Gravit. Cosmol.* **92**, 123516 (2015).
16. A. J. Cuesta, L. Verde, A. Riess, R. Jimenez, *Mon. Not. R. Astron. Soc.* **448**, 3463–3471 (2015).
17. S. Suyu et al., *Astrophys. J.* **691**, 277–298 (2009).
18. L. Koopmans, T. Treu, C. Fassnacht, R. Blandford, G. Surpi, *Astrophys. J.* **599**, 70–85 (2003).
19. C. Fassnacht, E. Xanthopoulos, L. Koopmans, D. Rusin, *Astrophys. J.* **581**, 823–835 (2002).
20. S. Suyu et al., *Astrophys. J.* **766**, 70 (2013).
21. M. Tewes et al., *Astron. Astrophys.* **556**, A22 (2013).
22. D. Sluse et al., *Astron. Astrophys.* **406**, L43–L46 (2003).
23. S. Refsdal, *Mon. Not. R. Astron. Soc.* **128**, 307–310 (1964).
24. V. Bonvin et al., *Mon. Not. R. Astron. Soc.* **465**, 4914–4930 (2017).
25. A. G. Riess et al., *Astrophys. J.* **855**, 136 (2018).
26. N. Aghanim et al., Planck 2018 results. VI. Cosmological parameters. arXiv:1807.06209 [astro-ph.CO] (17 July 2018).
27. D. Paraficz, J. Hjorth, *Astron. Astrophys.* **507**, L49–L52 (2009).
28. S. Suyu et al., *Astrophys. J.* **711**, 201–221 (2010).
29. S. Suyu et al., *Astrophys. J.* **788**, L35 (2014).
30. L. P. Osipkov, Spherical systems of gravitating bodies with an ellipsoidal velocity distribution. *Pisma v Astronomicheskii Zhurnal* **5**, 77–80 (1979).
31. D. Merritt, *Astron. J.* **90**, 1027 (1985).
32. E. Churazov et al., *Mon. Not. R. Astron. Soc.* **404**, 1165 (2010).
33. A. Agnello, N. W. Evans, A. J. Romanowsky, *Mon. Not. R. Astron. Soc.* **442**, 3284–3298 (2014).
34. Materials and methods are available as supplementary materials.
35. T. E. Collett et al., *Science* **360**, 1342–1346 (2018).
36. S. Hilbert, J. Hartlap, S. D. M. White, P. Schneider, *Astron. Astrophys.* **499**, 31–43 (2009).
37. M. Betoule et al., *Astron. Astrophys.* **568**, A22 (2014).
38. B. Audren, J. Lesgourgues, K. Benabed, S. Prunet, *JCAP* **2013**, 001 (2013).
39. D. Sluse et al., *Mon. Not. R. Astron. Soc.* **470**, 4838–4857 (2017).
40. C. E. Rusu et al., *Mon. Not. R. Astron. Soc.* **467**, 4220–4242 (2017).
41. K. C. Wong et al., *Mon. Not. R. Astron. Soc.* **465**, 4895–4913 (2017).
42. B. F. Schutz, *Nature* **323**, 310–311 (1986).
43. LIGO Scientific Collaboration and The Virgo Collaboration; 1M2H Collaboration; Dark Energy Camera GW-EM Collaboration and the DES Collaboration; DLT40 Collaboration; Las Cumbres Observatory Collaboration; VINROUGE Collaboration; MASTER Collaboration, *Nature* **551**, 85–88 (2017).

ACKNOWLEDGMENTS

We thank the HOLICOW and COSMOGRAIL collaborations for providing access to the observational data. We thank S. Birrer for comments that helped making the analysis more thorough and complete. We thank A. Sonnenfeld and M. Auger for providing their velocity dispersion code. We also thank A. Yıldırım for assistance with the Jeans Anisotropic Model code. **Funding:** S.H.S. thanks the Max Planck Society for support through the Max Planck Research Group. C.D.F. acknowledges support from the National Science Foundation grant AST-1312329. S.H. acknowledges support by the DFG cluster of excellence ‘Origin and Structure of the Universe’ (www.universe-cluster.de). L.V.E.K. is supported in part through an NWO-VICI career grant (project no. 639.043.308). **Author contributions:** All authors participated in the design of the experiment, the interpretation of the data, and the writing of the manuscript. I.J. performed the dynamics modeling and statistical analysis for inferring D_d , the inverse distance ladder analysis combining the JLA SNe with the lensing distances, and drafting and revising the manuscript. S.H.S. performed the lens mass modeling using the lensing and time-delay data, Bayesian statistical modeling combining the kinematic dataset with the lensing, and time-delay and external convergence datasets for inferring D_d , and assisted in the dynamic modeling of the lens. E.K. conceived and oversaw this research project. C.D.F. was the principal investigator of the observing programs that obtained the Hubble Space Telescope (HST) imaging of B1608+656 and the Keck spectroscopy for both lens systems and led the acquisition and initial reduction of those data. S.H. obtained and analyzed simulation data for the external convergence estimation. L.V.E.K. contributed to the HST and kinematics datasets and their analyses, the lensing and

kinematic modeling of the presented lenses, the interpretation of the results, and comments on the manuscript. **Competing interests:** The authors have no competing interests. **Data and materials availability:** The Hubble imaging data are available at the Hubble Legacy Archive <https://archive.stsci.edu/hst/search.php> under Proposal IDs 10158 (PI: Fassnacht), 7422 (PI: Readhead), and 9744 (PI: Kochanek). All the other data, e.g., the velocity dispersion, are available in the manuscript,

supplementary materials, or the references therein. The scripts and input files used for our analysis are available at <https://github.com/jee1213/ScienceInvDistLadder>. Our output cosmological parameters are listed in tables S1 and S2, with more details available with the scripts. To compute the velocity dispersions, we used codes developed by M. Auger and A. Sonnenfeld, available at https://github.com/astrosonnen/spherical_jeans.

SUPPLEMENTARY MATERIALS

science.sciencemag.org/content/365/6458/1134/suppl/DC1
Materials and Methods
Tables S1 and S2
Figs. S1 to S5
References (44–64)
10 April 2018; accepted 30 July 2019
10.1126/science.aat7371

A measurement of the Hubble constant from angular diameter distances to two gravitational lenses

Inh Jee, Sherry H. Suyu, Eiichiro Komatsu, Christopher D. Fassnacht, Stefan Hilbert and Léon V. E. Koopmans

Science **365** (6458), 1134-1138.
DOI: 10.1126/science.aat7371

Lensing approach to the Hubble constant

The current expansion rate of the Universe is parametrized by the Hubble constant, H_0 . Different methods of measuring H_0 produce results that disagree with each other, which could be a sign of new physics or of systematic errors in the methods. Jee *et al.* have analyzed two gravitational lensing systems to determine their distances (see the Perspective by Davis). They use these as benchmarks for a measurement of H_0 . The precision is not sufficient to resolve the debate but does bypass some of the systematic uncertainties. Observations of more lensing systems will be required to narrow down the value of H_0 .

Science, this issue p. 1134; see also p. 1076

ARTICLE TOOLS	http://science.sciencemag.org/content/365/6458/1134
SUPPLEMENTARY MATERIALS	http://science.sciencemag.org/content/suppl/2019/09/11/365.6458.1134.DC1
RELATED CONTENT	http://science.sciencemag.org/content/sci/365/6458/1076.full
REFERENCES	This article cites 61 articles, 2 of which you can access for free http://science.sciencemag.org/content/365/6458/1134#BIBL
PERMISSIONS	http://www.sciencemag.org/help/reprints-and-permissions

Use of this article is subject to the [Terms of Service](#)

Science (print ISSN 0036-8075; online ISSN 1095-9203) is published by the American Association for the Advancement of Science, 1200 New York Avenue NW, Washington, DC 20005. The title *Science* is a registered trademark of AAAS.

Copyright © 2019 The Authors, some rights reserved; exclusive licensee American Association for the Advancement of Science. No claim to original U.S. Government Works